

Electronic Supplementary Information

The Investigation of Methane Storage at the Ni-MOF-74

Material: A Periodic DFT calculation

Chen-Hao Yeh,^{a,b,c} Abdul Hannan Khan,^a Tsuyoshi Miyazaki,^{b,*} and Jyh-Chiang

Jiang^{a,*}

^aDepartment of Chemical Engineering, National Taiwan University of Science and
Technology, Taipei 10607, Taiwan

^bFirst-Principles Simulation Group, Nano-Theory Field, International Center for
Materials Nanoarchitectonics (WPI-MANA), National Institute for Materials Science
(NIMS), 1-1 Namiki, Tsukuba, Ibaraki 305-0044, JAPAN

^cDepartment of Materials Science and Engineering, Feng Chia University, No. 100,
Wenhwa Rd., Seatwen, Taichung, 40724, Taiwan

*Corresponding author. E-mail: MIYAZAKI.Tsuyoshi@nims.go.jp (T. Miyazaki)

*Corresponding author. E-mail: jcjiang@mail.ntust.edu.tw (J.-C. Jiang)

Thermodynamic correction

To include the temperature effect in this work, we carried out the thermodynamic correction of gaseous methane molecule and its adsorption on the Ni-MOF-74,

$$\Delta G = \Delta H - T\Delta S \quad (1)$$

$$G_i^0 = H_i^0 - TS_i^0 \quad (2)$$

in which ΔG , ΔH , and ΔS is the Gibbs free energy change, enthalpy change, and entropy change of the system, respectively; G_i^0 , H_i^0 and S_i^0 are molar Gibbs energy, molar enthalpy, and molar entropy of species i , respectively. The molar enthalpy can be composed as a sum of $E_{el,i}$ (electronic energy at 0 K), $E_{zpe,i}$ (zero-point vibrational energy), $E_{th,i}$ (thermal energy, including translational, rotational, vibrational, and electronic) and $PV_{m,i}$ work, as shown in eqn. (3)

$$H_i^0 = E_{el,i} + E_{zpe,i} + E_{th,i} + PV_{m,i} \quad (3)$$

For gaseous species, the thermodynamic properties include the translational, rotational and vibrational modes ($PV_{m,i}$ work can be replaced by RT , assuming an ideal gas). For H_i^0 of the gaseous species as a function of temperature, the zero-point energy correction and vibrational energy can be calculated as following,

$$E_{zpe,i} + E_{vib,i} = R \sum_k \left(\frac{\Theta_k}{2} + \frac{\Theta_k}{\exp(\Theta_k/T) - 1} \right) \quad (4)$$

in which $\Theta_k = hv_{i,k}/k_B$ is the vibrational temperature for vibrational frequency $v_{i,k}$ of species i , h is the Planck constant and k_B is the Boltzmann constant. Furthermore, for gaseous species moving in the three-dimensional space, the translational energy is $3/2 RT$, while the rotational energy, $3/2 RT$ for nonlinear. Consequently, for a nonlinear molecule, the H_i^0 of the gaseous species as a function of temperature is

$$\begin{aligned}
H_i^0 &= E_{zpe,i} + E_{vib,i} + E_{trans,i} + E_{rot,i} + PV_{m,i} \\
&= R \sum_k \left(\frac{\Theta_k}{2} + \frac{\Theta_k}{\exp(\Theta_k/T) - 1} \right) + 4RT
\end{aligned} \tag{5}$$

For S_i^0 of the gaseous species, which also include the translational, rotational, and vibrational contributions to the entropy, we calculated the translational, rotational, and vibrational entropy via their corresponding partition functions. The translational and rotational partition functions were obtained from the Gaussian 09 software by using the hybrid functional B3LYP and the 6-31G(d,p) basis set.¹ The translational and rotational entropy for the gas species can be calculated by the following equations:

$$S_{trans}^0 = R(\ln(q_{trans}) + 1 + 3/2) \tag{6}$$

$$S_{rot}^0 = R(\ln(q_{rot}) + 3/2) \tag{7}$$

The vibrational entropy can be obtained via calculating the vibrational frequencies and the following equation:

$$S_{vib}^0 = R \sum_k \left(\frac{\Theta_k/T}{\exp(\Theta_k/T) - 1} - \ln [1 - \exp(-\Theta_k/T)] \right) \tag{8}$$

For a nonlinear molecule, the S_i^0 of the gaseous species as a function of temperature is

$$S_i^0 = S_{vib,i} + S_{trans,i} + S_{rot,i} \tag{9}$$

In addition, both vibrational enthalpy and entropy need the vibrational frequency, however, since the current version of the CONQUEST code cannot compute vibrational frequencies, we adopted the VASP software²⁻⁵ to compute the vibrational frequency from the CONQUEST optimized geometries to calculate the thermodynamic corrections. In the calculation of VASP, the exchange and correlation energies were also computed within the GGA using the PBE functional and a kinetic energy cutoff of

400 eV. Ion-electron interactions were described by the projector augmented wave (PAW) formalism.⁶

For the adsorption species, the $PV_{m,i}$ term is ignored because the molar volume of surface species is negligible and rotational modes also make a small contribution, neither the translational modes; only vibrational modes for the internal energy contribution of the adsorbed species were considered (see eqn. (10)); similarly, S_i^0 for the adsorbed species (see eqn. (11)) was also calculated with only vibrational modes (translational and rotational modes can be ignored).

$$H_i^0 \approx E_{zpe,i} + E_{th,i} = R \sum_k \left(\frac{\Theta_k}{2} + \frac{\Theta_k}{\exp(\Theta_k/T) - 1} \right) \quad (10)$$

$$S_i^0 \approx S_{vib}^0 = R \sum_k \left(\frac{\Theta_k/T}{\exp(\Theta_k/T) - 1} - \ln [1 - \exp(-\Theta_k/T)] \right) \quad (11)$$

To simulate the adsorption isotherm, we adopted the dual-site Langmuir isotherm model as proposed by Alonso et al.⁷ for the different adsorption sites defined in this article, iSUB, L, and P sites. By using the modified Langmuir isotherm model, each adsorption site for its coverage is assumed to be a single Langmuir isotherm with a corresponding equilibrium constant. The sum of three individual Langmuir isotherms is the total coverage (θ) for the system. Hence, the coverage can be divided into three individual coverages of (1) the coverage at iSUB sites (θ_{iSUB}), (2) the coverage at the Linker sites (θ_L), and (3) the coverage at the pore sites (θ_{pore}). The total coverage represents the individual three coverages multiplied by the site distribution $\chi_i = N_i/N_{tot}$, where i means iSBU, L, or pore sites and N_{tot} is the total number of sites. The equilibrium constant can be solved by the calculated Gibbs free energy, and then the total coverage can be written as follows formula:

$$\theta = \chi_{iSBU} \theta_{iSBU} + \chi_L \theta_L + \chi_{pore} \theta_{pore}$$

$$= \chi_{iSBU} \frac{K_{iSBU}(\theta)P}{1 + K_{iSBU}(\theta)P} + \chi_L \theta_L \frac{K_L(\theta)P}{1 + K_L(\theta)P} + \chi_{pore} \theta_{pore} \frac{K_{pore}(\theta)P}{1 + K_{pore}(\theta)P} \quad (12)$$

Table S1. The comparison of the calculated bond lengths and bond angles of the Ni-MOF-74 structure with the experimental crystal data.

	Experiment	Calculation
d(C-H)	1.13	1.10
d(C-C)	1.48	1.45
d(C=C)	1.40	1.39
d(C-O)	1.29	1.28
d(Ni-O)	1.90	1.99
\angle (C-C-C) of linker	120°	119.97°
\angle (O-C-O) of linker	119.96°	119.74°
\angle (O-C-C) of linker	120.14°	121.48°
\angle (O-Ni-O) of iSBU (square planner)	89.97°	91.38°
\angle (O-Ni-O) of iSBU (octahedron)	90.84°	89.54°

Table S2. Calculated stepwise adsorption energy of 1 to 16 CH₄ on the Ni-MOF-74 without the BSSE correction, without the dispersion, and the dispersion energy.

Loading	E_{ads} (kJ/mol) w/o BSSE	E_{ads} (kJ/mol) w/o dispersion	E_{disp} (kJ/mol)
1	-32.58	-6.18	-16.44
2	-30.37	-5.03	-17.89
3	-27.62	-4.08	-15.86
4	-29.81	-5.10	-16.64
5	-29.96	-6.00	-16.22
6	-31.68	-5.57	-17.02
7	-43.62	-13.10	-17.82
8	-44.80	-8.88	-24.71
9	-41.00	-10.35	-18.74
10	-47.39	-11.33	-22.23
11	-41.88	-7.28	-22.33
12	-41.63	-4.47	-26.22
13	-23.42	-4.03	-14.32
14	-34.37	0.00	-23.04
15	-25.10	0.00	-10.53
16	-28.06	0.00	-11.02

Table S3. Calculated average adsorption energy of 1 to 16 CH₄ on the Ni-MOF-74.

Loading	^a E _{ads} (average) (kJ/mol)
1	-22.62
2	-22.77
3	-21.83
4	-21.81
5	-21.89
6	-22.01
7	-23.28
8	-24.57
9	-25.07
10	-25.92
11	-26.25
12	-26.62
13	-25.99
14	-25.78
15	-24.76
16	-23.90

^aThe average adsorption energy is calculated by using the following formula:

$$E_{\text{ads}} (\text{average}) = (E_{\text{tot}}[\text{MOF} + n\text{CH}_4] - E_{\text{tot}}[\text{MOF}] - nE_{\text{tot}}[\text{CH}_4])/n$$

Where $E_{\text{tot}}[\text{MOF} + n\text{CH}_4]$ represents the total energy of the Ni-MOF-74 framework after $n\text{CH}_4$ ($n=1\sim 16$) molecules adsorption. $E_{\text{tot}}[\text{MOF}]$ represents the total energy of the Ni-MOF-74 framework, and $E_{\text{tot}}[\text{CH}_4]$ is the total energy of the CH₄ molecule in vacuum; n is the numbers of methane molecules.

Table S4. Calculated stepwise adsorption Gibbs free energy of 1 to 16 CH₄ on the Ni-MOF-74 at different Temperatures.

Loading	G_{ads} (kJ/mol) 125K	G_{ads} (kJ/mol) 270K	G_{ads} (kJ/mol) 323K
1	-7.29	7.38	11.19
2	-7.59	7.08	10.89
3	-4.61	10.06	13.87
4	-6.41	8.26	12.07
5	-6.89	7.78	11.59
6	-7.26	7.41	11.22
7	-15.59	-0.92	2.89
8	-18.26	-3.59	0.22
9	-13.76	0.91	4.72
10	-18.23	-3.56	0.25
11	-14.28	0.39	4.20
12	-15.36	-0.69	3.12
13	-3.02	11.65	15.46
14	-7.71	6.96	10.77
15	4.80	19.47	23.28
16	4.31	18.98	22.79

Table S5. Calculated average adsorption Gibbs free energy of 1 to 16 CH₄ on the Ni-MOF-74 at different Temperatures.

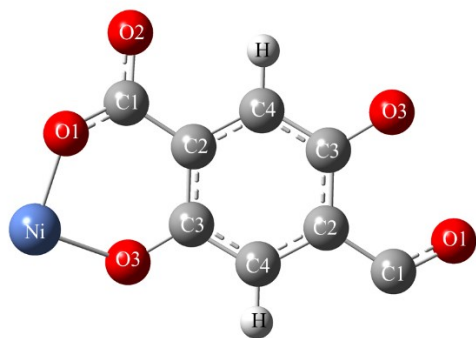
Loading	G_{ads} (kJ/mol) 125K	G_{ads} (kJ/mol) 270K	G_{ads} (kJ/mol) 323K
1	-7.29	7.38	11.19
2	-7.44	7.23	11.04
3	-6.50	8.17	11.98
4	-6.48	8.19	12.00
5	-6.56	8.11	11.92
6	-6.68	7.99	11.80
7	-7.95	6.72	10.53
8	-9.24	5.43	9.24
9	-9.74	4.93	8.74
10	-10.59	4.08	7.89
11	-10.92	3.74	7.55
12	-11.29	3.37	7.18
13	-10.66	4.01	7.82
14	-10.45	4.22	8.03
15	-9.43	5.24	9.05
16	-8.57	6.10	9.91

Table S6. Calculated partial charges of the framework in the present work in comparison with the previous works.^{8,9} (The labels of different atoms correspond to the labels in the following picture)

	^a Partial charge e	^b Partial charge e
Ni	1.298	0.868
O1	-0.789	-0.390
O2	-0.696	-0.384
O3	-0.785	-0.536
C1	0.895	0.276
C2	-0.349	-0.044
C3	0.418	0.174
C4	-0.173	-0.030
H	0.181	0.009

^a The values were taken from the works of Becker et al. and Lee et al.^{8,9}

^b The values were calculated in the present work.



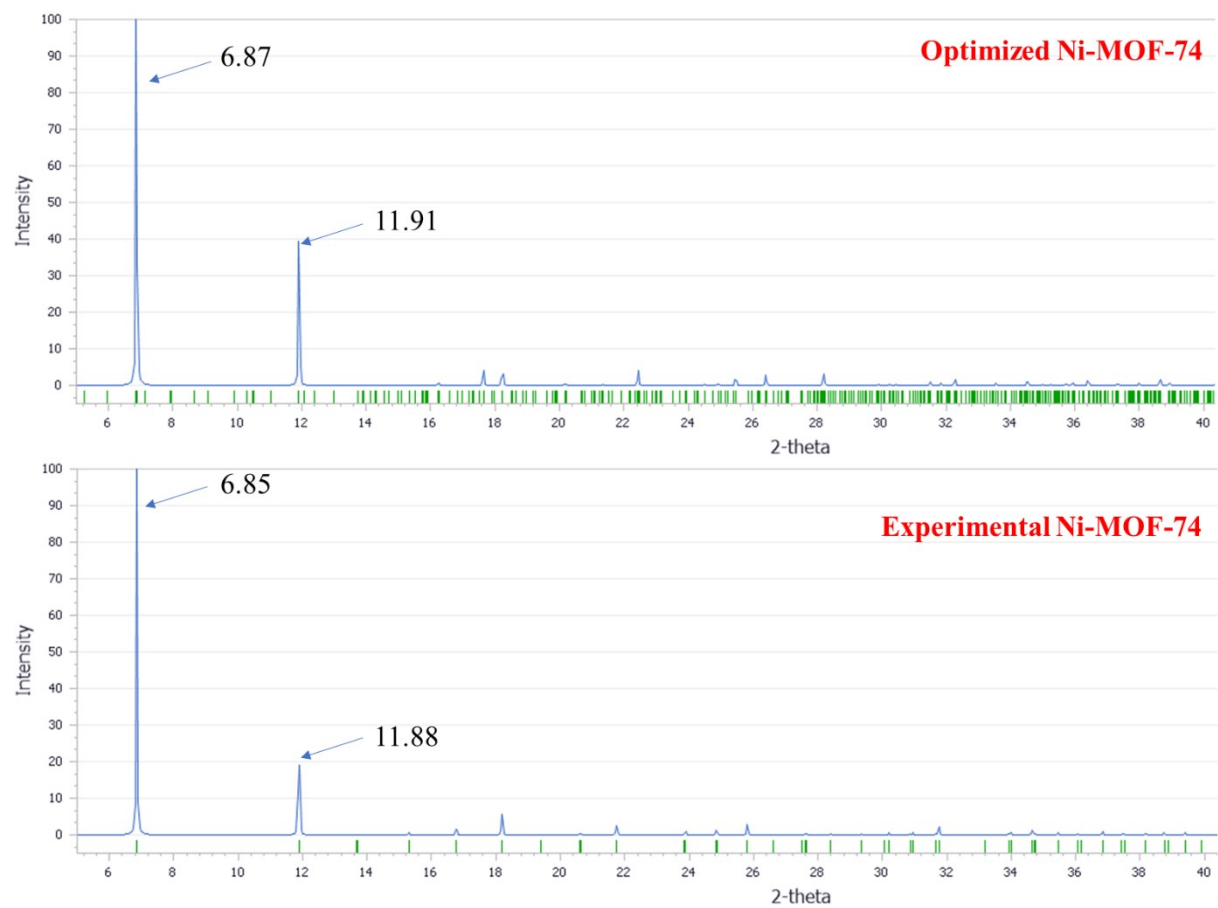


Figure S1. Calculated XRD patterns for the (upper) optimized Ni-MOF-74 and (bottom) the experimental cif data of the Ni-MOF-74. The experimental cif data is taken from ref 19.

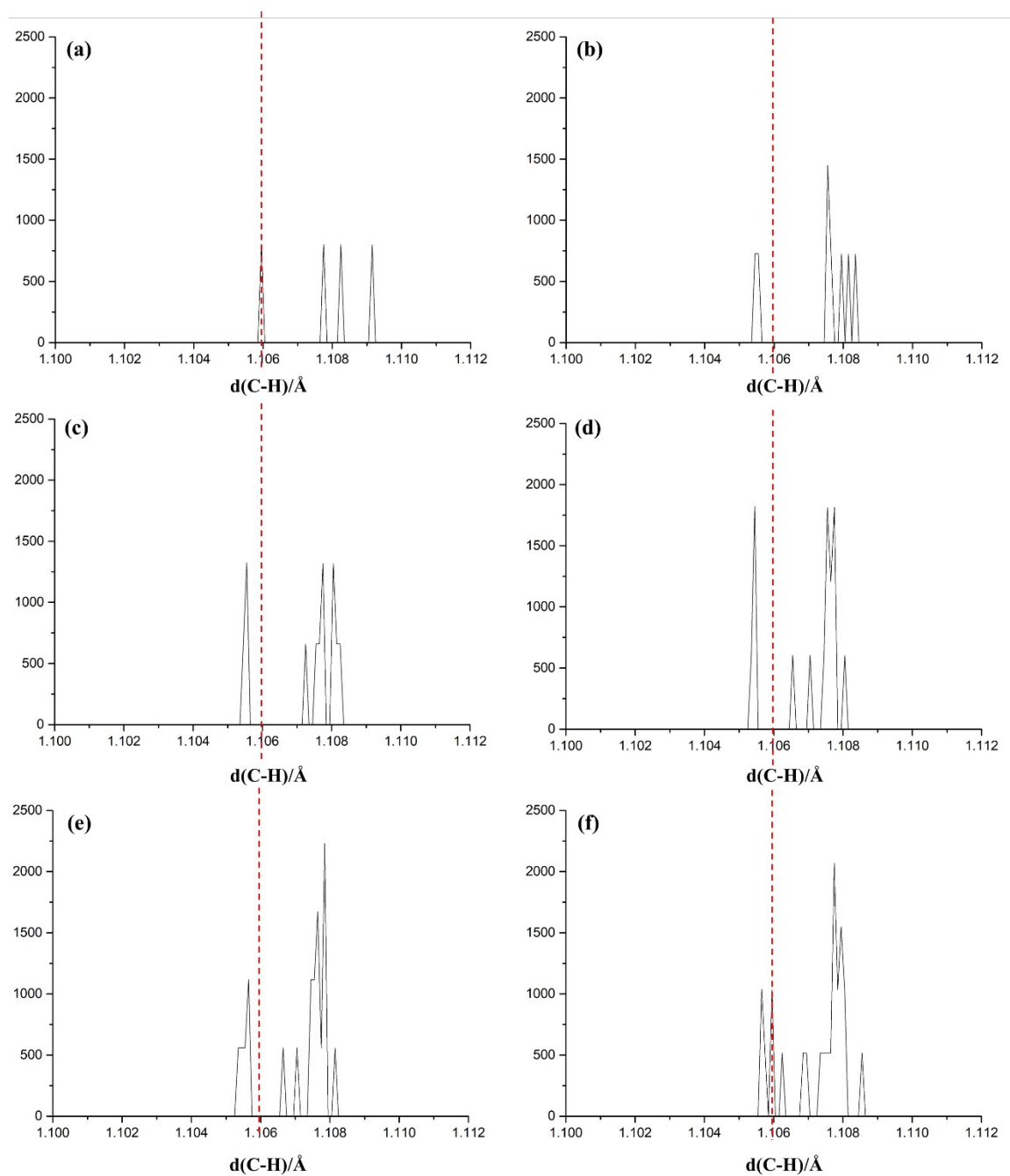


Figure S2. Calculated C-H bond distribution of multiple methane molecules adsorption on the Ni-MOF-74: (a) 1 CH₄, (b) 2 CH₄, (c) 3 CH₄, (d) 4 CH₄, (e) 5 CH₄, (f) 6 CH₄, (g) 7 CH₄, (h) 8 CH₄, (i) 9 CH₄, (j) 10 CH₄, (k) 11 CH₄, (l) 12 CH₄, (m) 13 CH₄, (n) 14 CH₄, (o) 15 CH₄, and (p) 16 CH₄. The dashed line represents the bond length of the free methane molecule (1.106 Å).

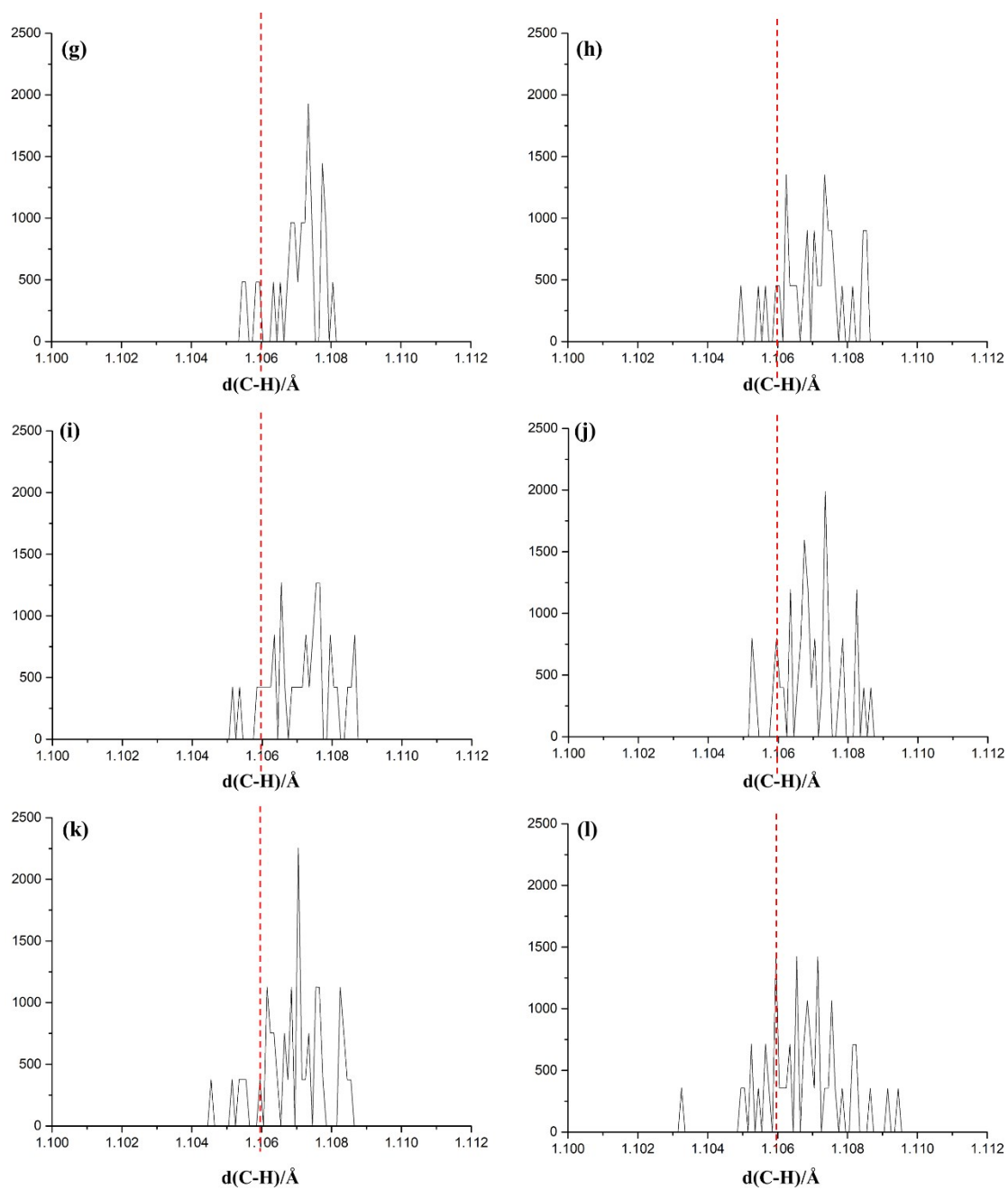


Figure S2 Continued.

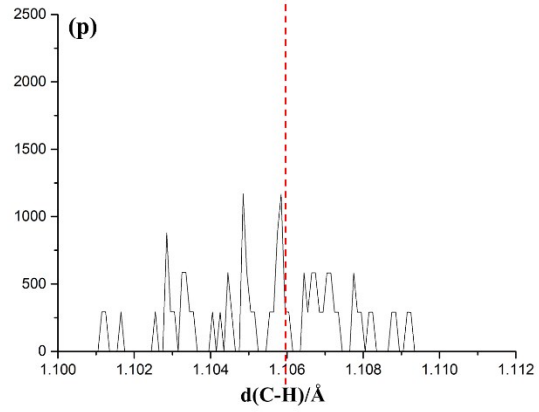
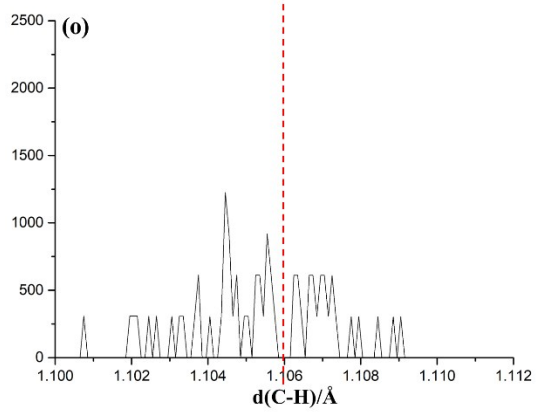
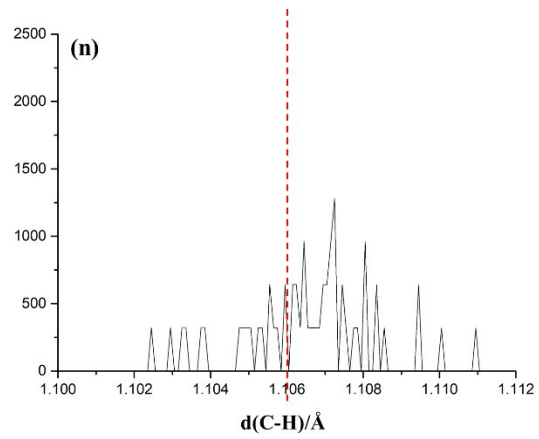
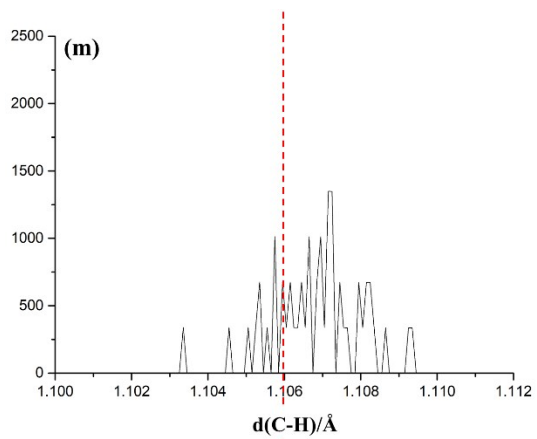


Figure S2 Continued.

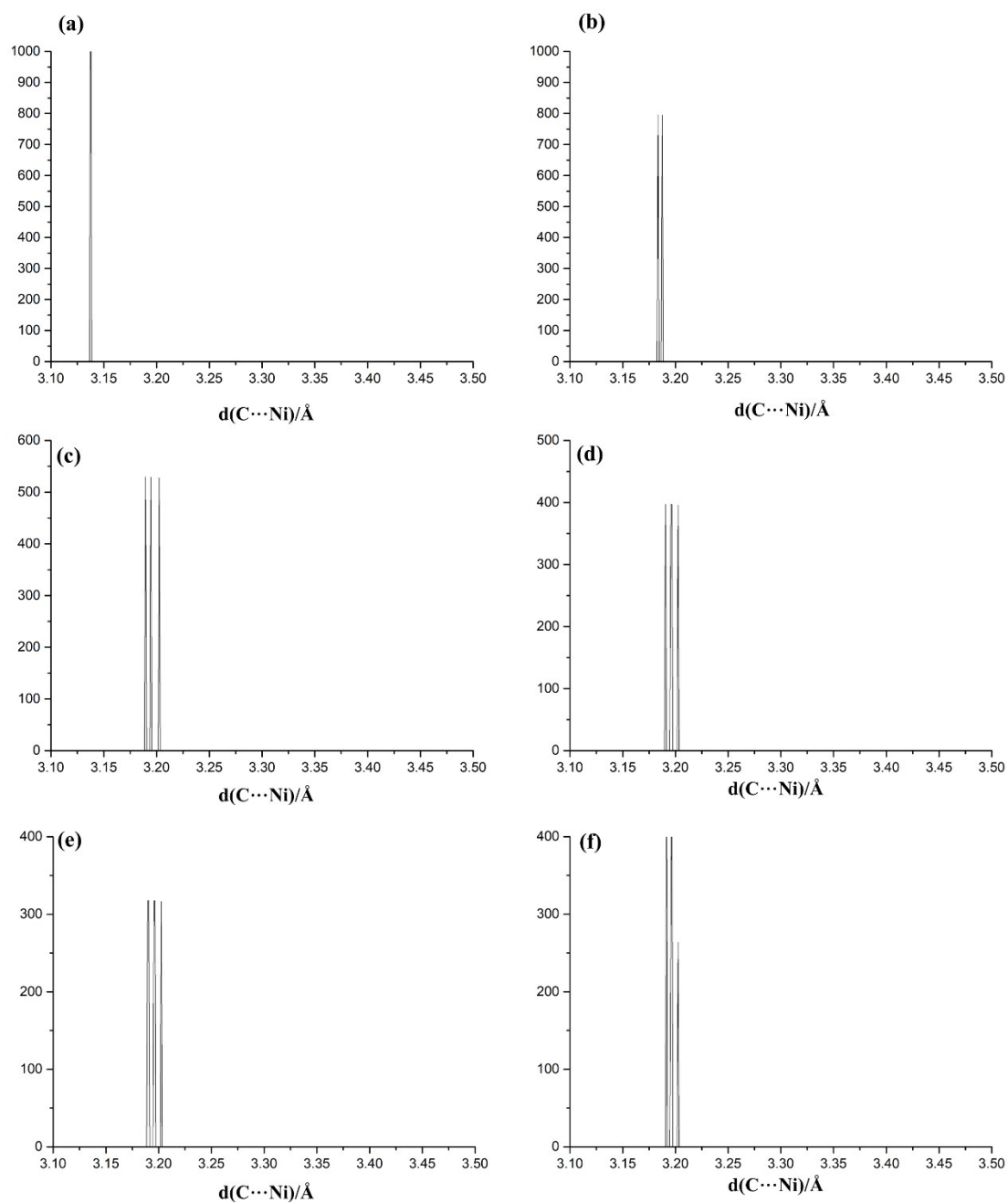


Figure S3. Calculated C...Ni bond distance distribution of multiple methane molecules adsorption on the Ni-MOF-74: (a) 1 CH_4 , (b) 2 CH_4 , (c) 3 CH_4 , (d) 4 CH_4 , (e) 5 CH_4 , (f) 6 CH_4 , (g) 7 CH_4 , (h) 8 CH_4 , (i) 9 CH_4 , (j) 10 CH_4 , (k) 11 CH_4 , and (l) 12 CH_4 .

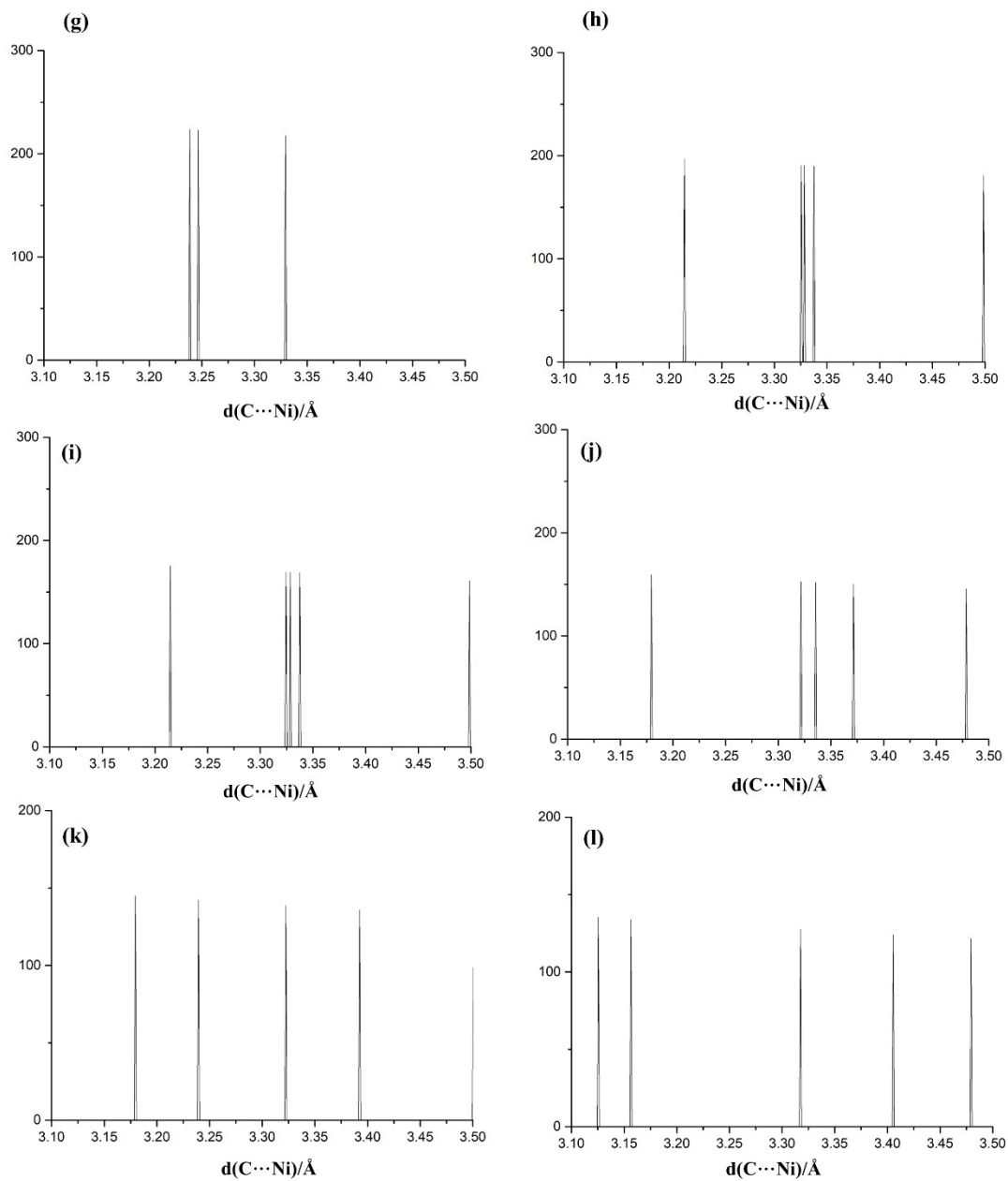


Figure S3 Continued.

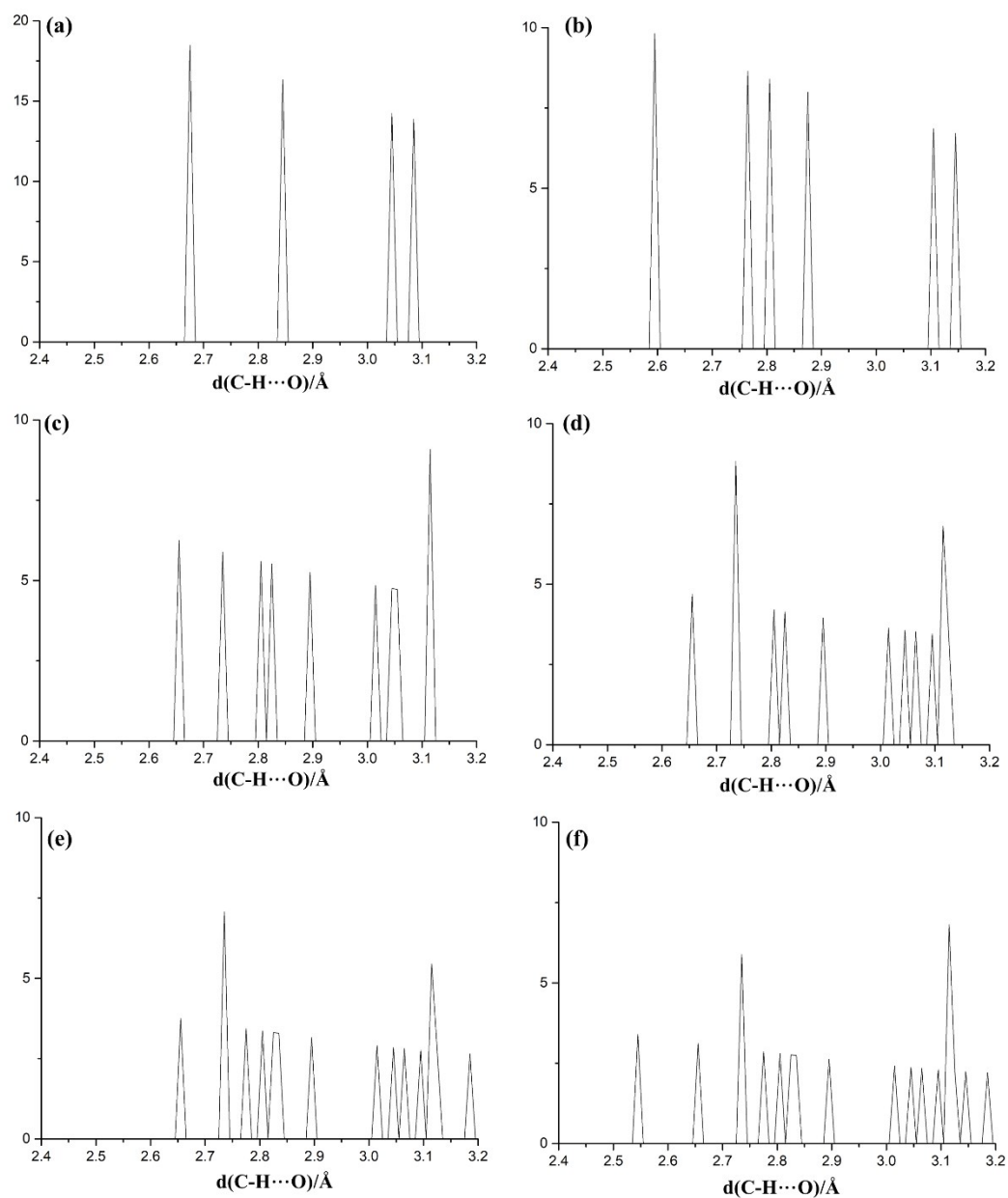


Figure S4. Calculated C-H...O bond distance distribution of multiple methane molecules adsorption on the Ni-MOF-74: (a) 1 CH₄, (b) 2 CH₄, (c) 3 CH₄, (d) 4 CH₄, (e) 5 CH₄, (f) 6 CH₄, (g) 7 CH₄, (h) 8 CH₄, (i) 9 CH₄, (j) 10 CH₄, (k) 11 CH₄, and (l) 12 CH₄.

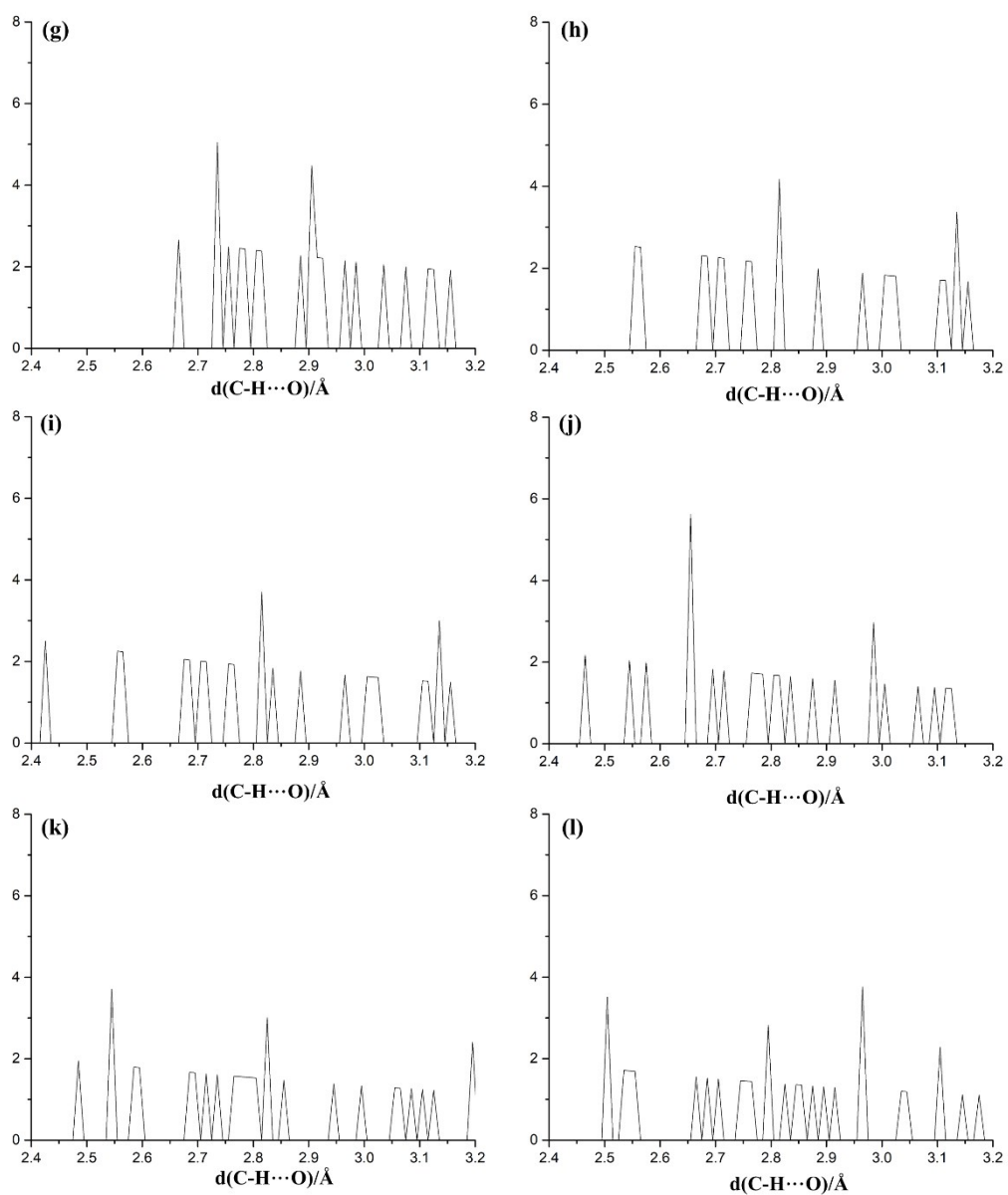


Figure S4 Continued.

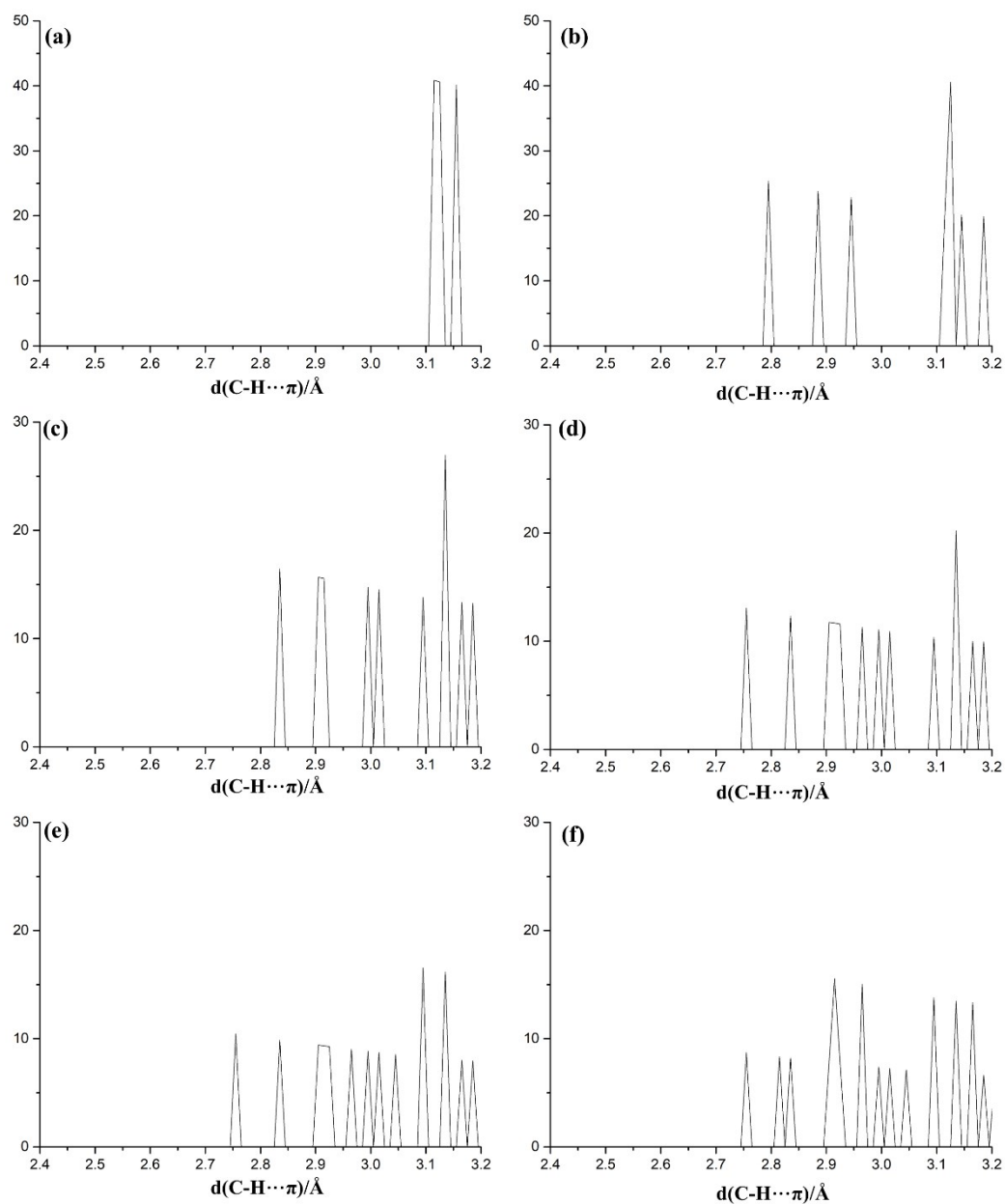


Figure S5. Calculated C-H... π distance distribution of multiple methane molecules adsorption on the Ni-MOF-74: (a) 1 CH₄, (b) 2 CH₄, (c) 3 CH₄, (d) 4 CH₄, (e) 5 CH₄, (f) 6 CH₄, (g) 7 CH₄, (h) 8 CH₄, (i) 9 CH₄, (j) 10 CH₄, (k) 11 CH₄, and (l) 12 CH₄.

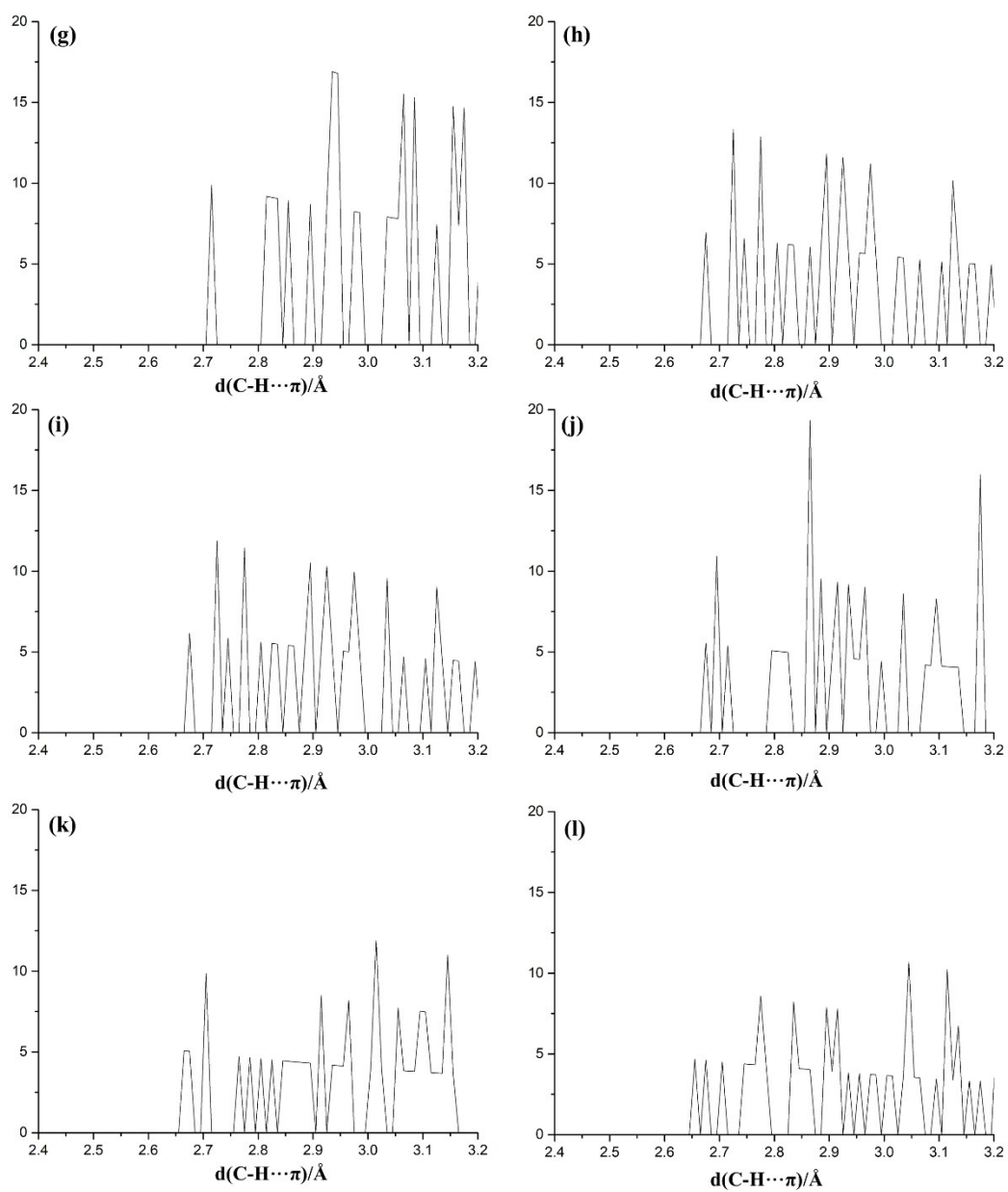


Figure S5 Continued.

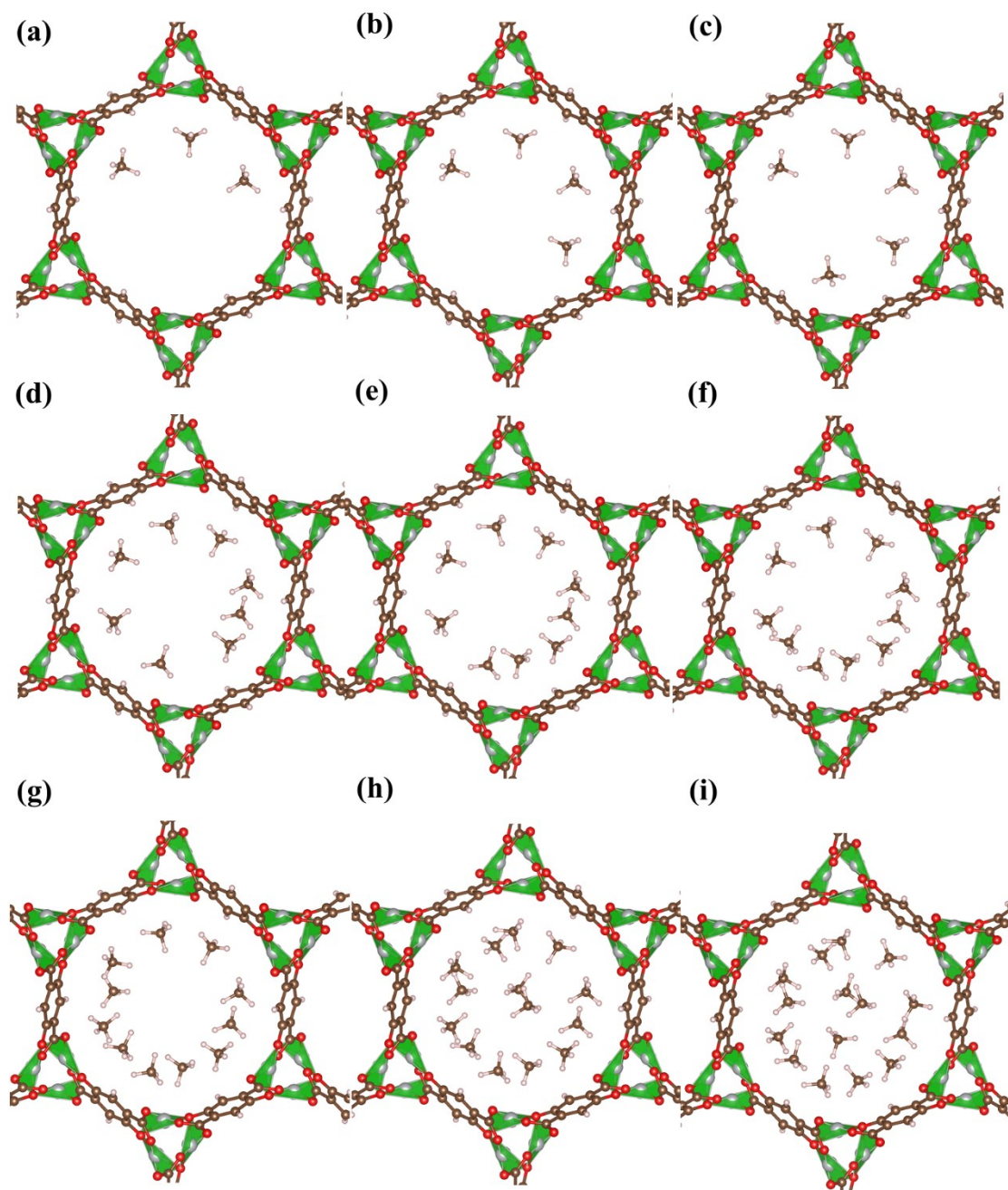


Figure S6. Optimized adsorption structures of multiple methane molecules in a pore of the Ni-MOF-74: (a) 3 CH₄, (b) 4 CH₄, (c) 5 CH₄, (d) 8 CH₄, (e) 9 CH₄, (f) 10 CH₄, (g) 11 CH₄, (h) 14 CH₄, and (i) 15 CH₄.

References

1. M. J. Frisch, G. W. Trucks, H. B. Schlegel, G. E. Scuseria, M. A. Robb, J. R. Cheeseman, G. Scalmani, V. Barone, B. Mennucci, G. A. Petersson, H. Nakatsuji, M. Caricato, X. Li, H. P. Hratchian, A. F. Izmaylov, J. Bloino, G. Zheng, J. L. Sonnenberg, M. Hada, M. Ehara, K. Toyota, R. Fukuda, J. Hasegawa, M. Ishida, T. Nakajima, Y. Honda, O. Kitao, H. Nakai, T. Vreven, J. A. Montgomery, Jr., J. E. Peralta, F. Ogliaro, M. Bearpark, J. J. Heyd, E. Brothers, K. N. Kudin, V. N. Staroverov, R. Kobayashi, J. Normand, K. Raghavachari, A. Rendell, J. C. Burant, S. S. Iyengar, J. Tomasi, M. Cossi, N. Rega, N. J. Millam, M. Klene, J. E. Knox, J. B. Cross, V. Bakken, C. Adamo, J. Jaramillo, R. Gomperts, R. E. Stratmann, O. Yazyev, A. J. Austin, R. Cammi, C. Pomelli, J. W. Ochterski, R. L. Martin, K. Morokuma, V. G. Zakrzewski, G. A. Voth, P. Salvador, J. J. Dannenberg, S. Dapprich, A. D. Daniels, O. Farkas, J. B. Foresman, J. V. Ortiz, J. Cioslowski, D. J. Fox, Gaussian 09, revision D. 01, Gaussian, Inc., Wallingford CT, 2013.
2. G. Kresse and J. Hafner, *Phys. Rev. B*, 1993, **47**, 558–561.
3. G. Kresse and J. Hafner, *Phys. Rev. B*, 1994, **49**, 14251–14269.
4. G. Kresse and J. Furthmuller, *J. Comp. Mater. Sci.*, 1996, **6**, 15–50.
5. G. Kresse and J. Furthmuller, *Phys. Rev. B*, 1996, **54**, 11169–11186.
6. G. Kresse and D. Joubert, *Phys. Rev. B*, 1999, **59**, 1758–1775.
7. G. Alonso, D. Bahamon, F. Keshavarz, X. Giménez, P. Gamallo and R. Sayós, *J. Phys. Chem. C.*, 2018, **122**, 3945-3957.
8. K. Lee, J. D. Howe, L.-C. Lin, B. Smit and J. B. Neaton, *Chemistry of Materials*, 2015, **27**, 668-678.
9. T. M. Becker, J. Heinen, D. Dubbeldam, L.-C. Lin and T. J. H. Vlugt, *The Journal of Physical Chemistry C*, 2017, **121**, 4659-4673.